Environmental Science & Technology

pubs.acs.org/est

Article

Top-Down Evaluation of Volatile Chemical Product Emissions Using a Lagrangian Framework

Bert W. D. Verreyken,* Colin Harkins, Meng Li, Wayne Angevine, Chelsea E. Stockwell, Lu Xu, Matthew Coggon, Jessica Gilman, Carsten Warneke, Edward Strobach, Steven Brown, Brandi McCarty, Richard Marchbanks, Sunil Baidar, Alan Brewer, Eva Y. Pfannerstill, Caleb Arata, Allen H. Goldstein, Jérome Brioude, and Brian C. McDonald

Cite This: *Environ. Sci. Technol.* 2025, 59, 7211−7221

Read Online

ACCESS | Metrics & More | Article Recommendations | Supporting Information

ABSTRACT: In this study, we evaluate volatile chemical product (VCP; e.g., adhesives, personal care products) emissions in the McDonald et al. inventory using sector-specific tracers and the FLEXPART-WRF Lagrangian particle dispersion model. Observations of decamethylcyclopentasiloxane (D5-Siloxane) are used for optimizing emissions from personal care products, para-dichlorobenzene (PDCBZ) for insecticides, and parachlorobenzotrifluoride (PCBTF) for emissions from the construction (coatings + adhesives) subsector. Continuous ground-site measurements obtained in Las Vegas and Los Angeles (LA) during summer 2021 are used to optimize the temporal emission profiles of the area sources. Additionally, in situ aircraft-based observations (June 2021) over the LA region are used to evaluate emission factors for the basin. The configuration of the weather research and forecasting (WRF) model is optimized using vertical wind profile measurements obtained from the Pick-Up truck-based Mobile Atmospheric Sounder (PUMAS) deployed in the LA basin to minimize the uncertainty of the inversion due to meteorology. While the diurnal amplitude in emission rates from personal care products and insecticides is reduced after optimization, that of construction VCPs (coatings + adhesives) is enhanced. From the aircraft inversion, we find that the inventory underestimates the emissions originating from construction by a factor of 5.3 (95% confidence interval 4.3−6.3) in the LA basin. Emissions from consumer products (personal care + cleaning) and insecticides were reduced by a factor of 2.1 (1.7−2.5) and 5.2 (3.9−6.4), respectively, following optimization.

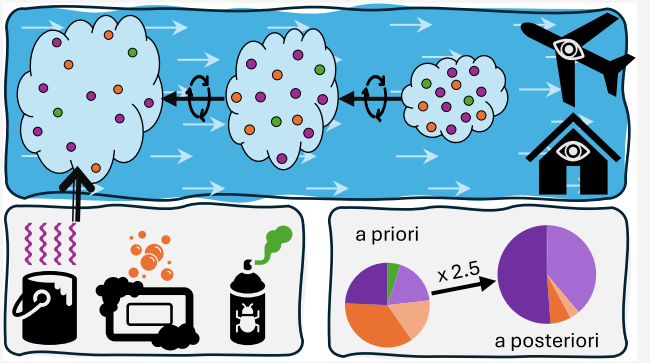

KEYWORDS: *emission inventory, volatile chemical products, top-down evaluation, diel emission patterns, air quality, in situ observations, southwestern USA*

INTRODUCTION

Volatile organic compounds (VOCs) are key in the formation of tropospheric ozone and serve as precursors to secondary organic aerosols (SOA). VOC emissions from anthropogenic activities were traditionally dominated by motor vehicles, whose emissions have steadily declined since the 1960s due to successful emission control measures.[2,3] In 2018, the use of volatile chemical products (VCPs) was identified as an emerging source of urban VOCs, accounting for half of the anthropogenic VOC reactivity and SOA formation potential in the Los Angeles (LA) basin during the summer of 2010.[1] Since then, measurements made in other cities, including New York City, confirmed their importance as sources of urban anthropogenic VOC emissions.[4,5] Gkatzelis et al. identified several VOC tracers for VCP emissions,[6] ubiquitous in US and European cities.[7] These include decamethylcyclopentasiloxane (D5-Siloxane) for personal care products, octamethylcyclotetrasiloxane (D4-Siloxane) for adhesives, para-dichlorobenzene (PDCBZ) for insecticides, and parachlorobenzotrifluoride (PCBTF) for solvent-borne coatings.[6] Using chemical transport modeling and box modeling, VCP emissions have been shown to enhance criteria air pollutants in urban regions over the US.[7−13] Estimates attribute 50−80% of emissions, reactivity, and SOA-forming potential of urban anthropogenic VOCs in the US to the use of VCPs.[4]

It is generally assumed that VCP emissions from consumer products correlate well with the population density. This was

Received: September 23, 2024
Revised: March 28, 2025
Accepted: March 28, 2025
Published: April 3, 2025

shown by mobile measurements in Europe and the US, which displayed high correlation between ambient VCP tracer concentrations and population density.[7] Furthermore, enhancement ratios of VCP tracers relative to tracers related to traffic emissions are elevated at locations with higher population density, thus illustrating a distinct source from traffic emissions.[4,6,7] A top-down evaluation comparing positive matrix factorization to emission sectors from the Fuel-based Inventory of Vehicular Emission with VCP emissions (FIVE-VCP[1,7,14,15]) found that the bulk source partition agreed to within 30% for the majority components.[4] Monoterpene emissions from anthropogenic inventories relative to biogenic emissions from the Model of Emissions of Gases and Aerosols from Nature (MEGAN[16]) corresponded better with source attribution in Atalanta (GA) when using FIVE-VCP than using the US Environmental Protection Agency's (EPA) National Emission Inventory (NEI) 2016v1 modeling platform.[17] Independent calculations for VCP emission factors (EFs) using the Stochastic Human Exposure and Dose Simulation (SHEDS) near-field tool[8] and the VCPy model[18] have been compared with the NEI and the McDonald et al.[1] inventories.[8,18] While the inventory by McDonald et al. was consistent with SHEDS,[8] the 2011 NEI underestimated national VCP emissions by a factor of 3−4. In contrast, VCPy was consistent with the 2017 NEI on a national level (though large differences were found regionally), while McDonald et al. was higher by a factor of ∼2.[18] Recently, a direct comparison between airborne VCP flux measurements over the LA basin and emission rates from inventories (FIVE-VCP and the California Air Resources Board (CARB) inventory) has identified discrepancies in both spatial emission patterns and total amount emitted.[19]

Past studies have focused on calculating VCP emission factors, evaluating the spatial variability of the absolute emissions, and comparing bulk VOC source attribution between inventories and matrix factorization techniques. While matrix factorization methods have been used to validate emission inventories by comparing the relative attributions to sector-based emissions (e.g., mobile sources vs VCPs), they have not been able to isolate subsector VCP factors (e.g., personal care products vs coatings).[4,17,20] In contrast, direct tracer-based studies to evaluate inventories should enable subsectoral attribution. Additionally, there is minimal information on the diel profiles of VCP emissions evaluated with atmospheric observations other than Coggon et al., who reported a diel pattern of personal care product emissions from ground-site data obtained in two North American cities (Boulder, CO; Toronto, ON, CA).[21]

In this work, we perform a top-down evaluation of VCP emissions in the McDonald et al. inventory using a mesoscale Lagrangian inversion framework. Lagrangian inversions are employed in a variety of optimization studies, e.g., evaluation of anthropogenic carbon monoxide (CO), nitrogen oxides (NO_x = NO + NO_2), and carbon dioxide (CO_2) emissions over California.[22] A Lagrangian model explicitly accounts for meteorological transport in an atmospheric inversion and is a traditional and computationally efficient approach to assessing bottom-up emission inventories at an urban subbasin scale, complementary to direct airborne eddy covariance fluxes. Evaluation of uncertainty in Lagrangian inversions is complex due to the convolution of uncertainties in meteorological fields, transport, source localization, chemistry, and deposition during transport. Inferred fluxes calculated with different Lagrangian models can diverge by a factor of 2 or more due to inconsistent vertical mixing.[23] However, differences between Lagrangian transport models do not provide a benchmark with reality and thus no clear error estimate is obtained by this approach.[24] Lagrangian forward simulations informed with ensemble meteorology to simulate transport from a known point source have been used to show that errors in Lagrangian transport models range from a few percent to over 100%.[24] These errors were dominated by inconsistencies in the wind field and the mixing layer height from the underlying meteorological model.[24] As a result, Angevine et al. advocated clear evaluation of the meteorological model and potentially a selection of observations coincident with periods where the model performs well in order to reduce model error.[24]

Here, inverse modeling is applied to the VCP tracers (defined by Gkatzelis et al.[6] to be measurable, long-lived, and predominantly emitted by one VCP subsector) to evaluate subsector emissions directly. We utilize ground-based measurements from the Southwest Urban NO_x and VOC Experiment (SUNVEx, https://csl.noaa.gov/projects/sunvex/; last access 8 Dec 2023) 2021 field campaign in Las Vegas (LV; July 2021) and LA (Aug 2021), and aircraft measurements from the Re-Evaluating the Chemistry of Air Pollutants in California (RECAP-CA; June 2021). Using meteorological measurements from the SUNVEx campaign, an inverse modeling framework, and in situ observations of VCP tracers, we aim to respond to the following questions:

- What setup of the meteorological model sufficiently represents the dynamics in the LA basin to describe region-specific mesoscale transport patterns for performing a Lagrangian inversion?
- Can continuous ground-site measurements be leveraged in combination with a Lagrangian framework to optimize the diel variability from subsector VCP emissions?
- Do emission factors accurately capture the magnitude of subsector VCP emissions in the LA basin?

To the best of the authors' knowledge, this is the first time a Lagrangian framework has been applied to evaluate subsector VCP emissions and their diel profiles.

METHODOLOGY

Modeling. *Numerical Weather Prediction Model.* Meteorological data to drive the Lagrangian model are obtained from the Weather Research and Forecasting model with chemistry (WRF-Chem v4.2). Twelve different model configurations were evaluated. Li et al.[25] documented the initial configuration used as a basis for this work. Using the base configuration, we introduced nested domains (SI Figure S6) to evaluate typical atmospheric chemistry modeling grid spacing (12, 4, and 1.3 km).[26−28] Additionally, we evaluated changing the model to provide the meteorological input for initial and boundary conditions (IC/BCs). The base configuration used the North American Mesoscale (NAM[29]) model for IC/BCs; alternatives tested were the Rapid Refresh (RAP[30]) and the High-Resolution Rapid Refresh (HRRR[30]) models. Finally, we optimized the physics configuration. The boundary layer (BL) scheme used in the base configuration is the Mellor−Yamada−Nakanishi−Niino (MYNN[31]) parametrization. We included the Eddy Diffusivity Mass Flux subparameterization (EDMF[32]) within the MYNN configuration and tested the use of a Single Layer Urban Canopy (SLUC[33]).

Lagrangian Transport Model. The FLEXible PARTicle dispersion model FLEXPART[34] is a Lagrangian particle

https://doi.org/10.1021/acs.est.4c10117
Environ. Sci. Technol. 2025, 59, 7211−7221

dispersion model (LPDM) that is frequently used to model atmospheric transport processes. Here, we will use the version compatible with WRF output, FLEXPART-WRF,[35] to evaluate subsector VCP emissions directly by performing inversions using their specific tracers. Different LPDMs have been shown to diverge in results even when using the same meteorological driving models, specifically due to differences in vertical dispersion parametrizations in the transport models.[23] FLEXPART-WRF was run with the boundary layer representation obtained from the turbulent kinetic energy (TKE) profiles in the WRF-Chem model. The TKE-driven mode in FLEXPART-WRF was adapted according to the method introduced in FLEXPART-AROME[36] with mixing length profiles retrieved directly from WRF-Chem. Hourly average winds are used as they have been shown to significantly reduce the uncertainty and bias of the model in complex terrain.[37] FLEXPART-WRF was run in backward mode[38] in order to obtain the footprint between the surface and 100 m above ground level (a.g.l.) for all observations. More details on the FLEXPART-WRF configuration and air mass representation are available in the SI (Sections S2 and S3).

Emission Inventory. We use a gridded VCP inventory described previously by McDonald et al. and Coggon et al.[1,7,39] The inventory was updated using near real-time scaling factors to represent emissions changes in 2019−2021, e.g., from COVID-19 lockdowns.[26] Use of VCPs, by mass, is calculated from a mass balance of US chemical product manufacturing in 2010[7,39] and updated with economic activity scaling factors developed from wholesale trade in chemical manufacturing for industrial VCP emissions and retail trade in Health and Personal products and Pharmacy and Drugstores for consumer product VCPs.[26] Emissions of VOCs from VCP use are calculated by applying emission factors (g VOC/g Product), nationally, to VCP subsectors (VCP US). Some regions, including LA, regulate the VOC content of chemical products more stringently, which is taken into account. The EPA 2017 NEI is used for emissions from other sectors and updated using near real-time scaling factors developed from publicly available economic and energy metrics applicable to emission subsectors.[26] Herein, we refer to the inventory as VCP US and VCP LA to indicate the use of national or regionally applied emission factors (kg person^{-1} year^{-1}). The emissions are then gridded based on US Census population counts. Lastly, we updated the VOC speciation profiles of VCPs based on the latest California Air Resources Board (CARB) data for 2020 (https://ww2.arb.ca.gov/speciation-profiles-used-carb-modeling; last access 15 July 2024).

Observations. *SUNVEx Ground-Site VOC Measurements.* The SUNVEx field campaign occurred in the summer of 2021 and measurements were taken in LV (6/30−7/27), and LA (8/7−9/7, 2021). The goal of the campaign was to measure ozone precursors and fill gaps in measuring VOCs not routinely monitored by air quality stations. Here, we focus on measurements made at the Jerome Mack Middle School ground site in LV (105.0787° W, 36.1418° N), and the California Institute of Technology ground site in LA (118.1256° W, 34.1403° N). VOCs were measured using a proton-transfer-reaction time-of-flight mass spectrometer (PTR-ToF-MS) as described by Coggon et al.[40] The PTR-ToF-MS sampled air at 1 L min^{-1} through a 10 m Teflon inlet and reported VOC mixing ratios on a 1 min average. All VOCs reported here (D4-Siloxane, D5-Siloxane, PDCBZ, and PCBTF) were calibrated using certified gas standards (Apel-Riemer Environmental Inc., Miami, FL) or by liquid calibration methods.[40]

SUNVEx Doppler Lidar Measurements. A ground-based stationary scanning Doppler lidar was deployed in LV (7/1−8/4), and Pasadena, CA (8/5−9/2), during the 2021 SUNVEx campaign to measure vertical and horizontal wind profiles, calculate vertical velocity variance (turbulence) profiles, and derive mixed layer height. The Doppler lidar made a set of conical scans 15, 35, and 60° elevation angles, which took ∼3.5 min, every 15 min, and stared vertically for the remainder of the 15 min cycle. Mean horizontal winds were derived from a set of conical scans and reported every 15 min. The vertical resolution of the wind profiles ranged from 20 m near the surface to 50 m above 3 km a.g.l. Vertical velocity measurements were used to calculate the vertical velocity variance, skewness, and kurtosis. Mixed layer height was derived from the Doppler lidar measurements using the fuzzy logic approach.[41]

The Pick-Up truck-based Mobile Atmospheric Sounder (PUMAS) made a series of drives in the LA basin starting and ending at Pasadena, CA. PUMAS is a microjoule class Doppler lidar which is actively motion stabilized during the drives and can be operated in either vertical stare mode for making vertical velocity measurements, or scanning mode for making horizontal wind profile measurements.[42] During SUNVEx, PUMAS made horizontal wind profile measurements at 60 m vertical resolution and 30 s time resolution. The horizontal resolution of the wind profiles varied with driving speed. PUMAS made a total of 18 drives, which were classified as (1) sea breeze drive extending to the Long Beach in the South, (2) basin survey from Santa Monica in the west to Redlands in the East, or (3) mountain drive up the San Gabriel mountains.

RECAP-CA Airborne VOC Measurements. Nine Navy Twin Otter flights were conducted over the LA Basin between June 1−22, 2021, at 300−400 m a.g.l. as part of the RECAP-CA campaign.[19,43−45] The 5 h long flights took place between 11:00 and 17:00 local time. VOC concentrations were measured by a Vocus PTR-ToF-MS.[46] VOCs were drawn from a ∼6 m long inlet sampling at the nose of the aircraft. Details on the climatology during the study as well as the VOC sampling and calibration can be found elsewhere.[45] The PTR-ToF-MS resolution was about 4800 with mass spectra recorded from 10 to 500 Da. In-flight zero-air measurements were subtracted. Ground calibrations were conducted every 1−3 days, using gravimetrically prepared multicomponent VOC standards (Apel-Riemer Environmental, Inc., Colorado). Among the VOCs discussed here, D4-Siloxane and D5-Siloxane were included in the gas standard. For all m/z without a corresponding gas standard, including PDCBZ and PCBTF, sensitivities were derived from a root function fit to reaction rate normalized sensitivities of nonfragmenting and nonclustering gas standard calibrated VOCs.[47] The estimated calibration uncertainty for D4- and D5-Siloxane was 20%, and for PDCBZ and PCBTF it was 54%.

Inversion Framework. Lagrangian particle dispersion models can be used in a backward mode to generate a source-receptor matrix (also called footprint) for observations.[38] The convolution of the footprint of an observation (H), with an emission inventory of a passive tracer (x) results in an estimated mixing ratio at the observation location (y^{est})

$$y_{i,j}^{est} = \sum_{k} \sum_{l} H_{i,k,l} \times x_{j,k,l} \quad (1)$$

https://doi.org/10.1021/acs.est.4c10117
Environ. Sci. Technol. 2025, 59, 7211−7221

where the indices i and j represent the observation time and species, respectively, and indices k and l represent time and location of emissions, respectively.[38] Here, we use the variational method as discussed by Brioude et al.[48] as a basis to optimize the diel and spatial emission distributions. In short, an optimal solution for x is obtained by minimizing the cost function (J) to converge to a solution quickly. Assuming log-normal distributions for observations and the prior inventory results in the following cost function[49]

$$J = J_{\text{obs}} + J_{\text{prior}}$$

$$= \frac{1}{2}(\ln y^{\text{Obs}} - \ln Hx)^T R^{-1}(\ln y^{\text{Obs}} - \ln Hx) + \frac{1}{2}(\ln x - \ln x_b)^T B^{-1}(\ln x - \ln x_b)$$

where y^{Obs} are the observed mixing ratios, x_b is the matrix containing the prior, and R and B are the error covariance matrices of the observations and the prior.

Temporal Inversion. We adapt the form of emission inventory x here to separate the temporal evolution in the emissions inventory (EI) from the spatial distribution. This is achieved through the decomposition of the EI

$$x'_{j,l} \equiv \sum_k x_{j,k,l},\ D_{j,k,l} \equiv \frac{x_{j,k,l}}{x'_{j,l}}$$

where $x'_{j,l}$ represents the total daily emissions at location l for species j, and $D_{j,k,l}$ the fraction of these total emissions at location l and time k for species j, respectively.

The diel distribution ($D_{j,k,l}$) from VCP LA is unique to location l and depends on the relative impact of area/point emissions of species j. However, the impact of point sources is negligible for the ground-based measurements so that $D_{j,k,l}$ is fully determined by the area source (i.e., location-independent) and we restructure eq 1 as follows

$$y^{\text{est}}_{i,j} = \sum_k y^{\text{est}}_{i,j,k} \times D_{j,k} \tag{2}$$

with

$$y^{\text{est}}_{i,j,k} = \sum_l H_{i,k,l} \times x'_{j,l} \times e^{-[\text{OH}]\times k_j \times \Delta t_{i,k}} \tag{3}$$

and $D_{j,k}$ the diel distribution of emissions from chemical compound j in time. Additionally, note that simple chemical decay is taken into account by the exponential function where k_j is the reaction rate constant for compound j, [OH] the average OH concentration (2.5×10^6 molec. cm^{-3}, within the range of model OH concentrations reported for a selection of the flights from RECAP-CA[43]), and $\Delta t_{i,k}$ the time between emission and observation. Here, $y^{\text{est}}_{i,j,k}$ serves as the equivalent of linear operator H in eq 1, while the diel profile can be optimized through minimizing the cost function.

VCP Emission Factors. As mentioned in the Introduction section, emission factors (EFs) differ up to a factor of 4 between different inventories[8,17,18] and do not match airborne emission observations.[19] This illustrates that the bottom-up inventory EFs are subject to high uncertainties. When we assume that both the temporal and spatial variability are reasonably well represented by the inventory, we can evaluate the EFs using the subsector tracer approach. By comparing expected mixing ratios for the different tracers (eq 1), with observations, we define a scaling factor by taking the ratio of y^{est} and y^{Obs}. Application of these scaling factors to the respective EF results in top-down EF estimates for subsector VOC emissions.

Spatial Inversion. When we update the emissions inventory by top-down EFs, we can use a spatial optimization to identify regions where emissions are not well represented. By updating the diel distribution in the area source and assuming that the point/area ratio is known for every point in the domain, we fix the diel profiles and restructure eq 1

$$y^{\text{est}}_{i,j} = \sum_l y^{\text{est}}_{i,j,l} \times x'_{j,l} \tag{4}$$

with

$$y^{\text{est}}_{i,j,l} = \sum_k H_{i,k,l} \times D_{j,k,l} \times e^{-[\text{OH}]\times k_j \times \Delta t_{i,k}} \tag{5}$$

Now, $y^{\text{est}}_{i,j,l}$ serves as the equivalent of the linear operator H while the total daily emissions can be optimized through minimization of the cost function.

Tracer Selection. Evolving VCP organic compound composition adds complications for identifying tracers for subsector emissions. When updating the speciation of VCP emissions to the most recent CARB 2020 profiles, we found that not all of the tracers identified by Gkatzelis et al. (D5-Siloxane, personal care; D4-Siloxane, adhesives (75%) and insecticides (25%); PCBTF, solvent-borne coatings; and PDCBZ, insecticides)[6] are representative for the 2021 emissions of specific subsectors in the emission inventory. While D5-Siloxane and PDCBZ remain unique tracers for personal care and insecticides, respectively, PCBTF is emitted predominantly by application of coatings (84.1%) and adhesives (15.2%), with small contributions from cleaning products (0.7%; neglected here). D4-Siloxane has been adapted significantly and is emitted by coatings (50%), personal care (31%), cleaning (16%), and insecticides (3%). As adhesives and coatings are chemically related (lower fraction of oxygenated compounds[1]) and emissions likely result from similar construction and building material-related activities, we redefine PCBTF as a tracer for construction-related (coatings + adhesives; from both commercial and household uses) emissions. Similarly, the chemical signature of personal care and cleaning products are predominantly oxygenated[1] and their use is likely driven by consumer activity patterns and coincident with one another. Here, we define D5-Siloxane as a tracer for consumer VCPs (personal care + cleaning). These definitions for construction and consumer tracers are consistent with findings by He et al. which observed drops in sales of health and personal care products while those of building materials increased, consistent with measurements of D5-Siloxane and PCBTF in Boulder, CO.[26]

Since D4-Siloxane is emitted across these three broader VCP subsector categories, we can check the inversion results. We do this by estimating D4-Siloxane emissions from adjusting VOC emissions from construction (coatings + adhesives), consumer VCPs (personal care + cleaning), and insecticides using PCBTF, D5-Siloxane, and PDCBZ, respectively. Then, we compare this derived estimate of D4-Siloxane to a direct atmospheric inversion of D4-Siloxane.

The remaining tracers identified by Gkatzelis et al. are not considered as their atmospheric lifetime is too short (below 1 day), which results in a significant portion being lost before measurement. In contrast, atmospheric lifetime for selected tracers is 4−5 days (assuming atmospheric OH concentrations of 10^6 molecules cm^{-3}) for D5-Siloxane, 6 days for D4-Siloxane, and over a month for PCBTF and PDCBZ. As we are unable to

https://doi.org/10.1021/acs.est.4c10117
Environ. Sci. Technol. 2025, 59, 7211−7221

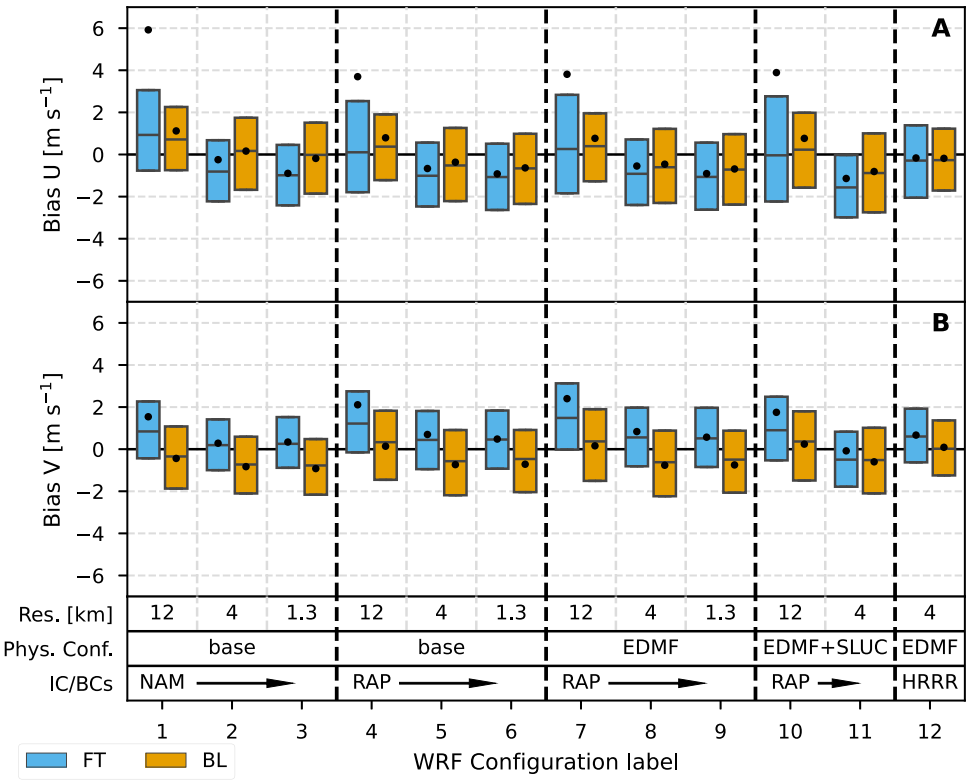

Figure 1. Biases in zonal (A) and meridional (B) wind directions for each WRF-Chem configuration using mobile Doppler lidar observations as a reference. The boxes illustrate the median and the interquartile range of the biases for each data point in the observations, the average bias is represented by the black dot. Biases were separated by Free Troposphere (FT; blue), and Boundary Layer (BL; orange) regions according to model boundary layer height. The lowest three rows document the WRF-Chem configuration describing, respectively, (i) the model used to provide initial and boundary conditions (IC/BCs; nested runs represented by arrows), (ii) the PBL configuration, and (iii) the horizontal grid spacing.

use the tracer for water-borne coating emissions (Texanol), we assume that the ratio between solvent-borne and water-borne coatings is reasonably distributed in the CARB inventory and speciation profiles.

RESULTS AND DISCUSSION

Meteorological Evaluation. Errors in Lagrangian transport models are dominated by inconsistencies in the wind field and the mixing layer height from the underlying meteorological model.[24] We optimize the model configuration and use the setup that best represents the dynamical observations during the SUNVEx campaign. Additionally, a careful selection of observations is done based on how well the model represents the boundary layer.

Twelve setups of the meteorological model are evaluated for their ability to reproduce horizontal winds obtained from the PUMAS instrument in LA. Hourly average model wind is interpolated in time and space to match the lidar observations, similar to what is done with FLEXPART-WRF. The interquartile range (IQR), median, and average of the model bias distributions for the different configurations (Figure 1) illustrate the expected uncertainties from the transport simulations. While the median and average value of the bias distribution are expected to tend toward 0 m s^{-1} for an unbiased model, the IQR will have a minimal value representative for subscale motions not resolved in the model output (e.g., turbulence). Comparisons of mesoscale transport processes between PUMAS and model configurations averaged across the vertical model grid can be viewed in the Supporting Information (e.g., SI Figures S1, S4, and S5).

In Figure 1, we see that the largest average biases are found for all of the simulations with 12 km grid spacing. This is due to the poor representation of mesoscale transport processes in this coarse grid. The highest impact on model performance is obtained when changing the horizontal grid spacing from 12 to 4 km. Overall, little meteorological improvement is obtained from going to finer than 4 km spacing in the LA domain. Local flows resulting from strong gradients in surface elevation may be better resolved in the 1.3 km runs (see SI Figures S4 and S5) though this is not expected to significantly affect results from the Lagrangian inversion here. The preferred configuration is found to be using HRRR as meteorological input with EDMF where the model bias in zonal (meridional) wind vector components is -0.18 ± 3.85 (0.30 ± 2.90) m s^{-1}. As a reference, variation in the observations is 3.00 (2.73) m s^{-1} for the zonal (meridional) directions and thus are consistent with the variation in model biases. The largest source of bias in wind direction for the selected configuration originates from the meridional direction in the free troposphere (0.67 ± 2.75 m s^{-1}). However, this is not expected to affect the inversion, which is dominated by transport within the boundary layer.

After optimizing the model configuration using wind profiles, we exclude data from the inversion, where we estimate that the boundary layer is not well reproduced in the model. For the ground-based sites, we use boundary layer height comparison between the model and the stationary lidar instrument. Inconsistent boundary layer representation between the model and measurements excludes 5 out of 24 (9 out of 21) days from our analysis in LA (LV) as shown in SI Figures S2 and S3. The average relative bias for daytime (8 a.m.−8 p.m. local time)

https://doi.org/10.1021/acs.est.4c10117
Environ. Sci. Technol. 2025, 59, 7211−7221

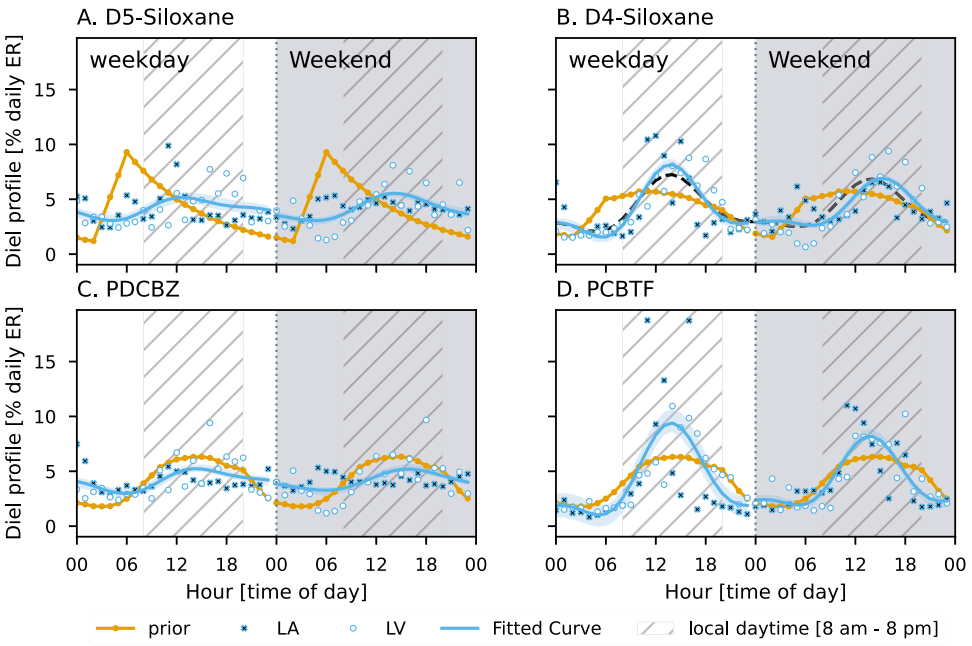

Figure 2. Diel profile (% of daily emission) as a function of time of the day for D5-Siloxane, D4-Siloxane, PDCBZ, and PCBTF (A–D, respectively). White (gray) background denotes weekday (weekend) days for each tracer. Gray hatched regions denote local daytime (8 a.m. to 8 p.m.). The orange curves are the prior for the area sources in the McDonald et al. inventory. Blue contoured black crosses (white dots) represent the inversion result for LV (LA) with second-order Fourier sum (fitted to both) shown as a blue curve. The std range of the fitted curve is shown as a blue-shaded area behind the curve. The dashed line in (B) shows the diurnal emission profile for D4-Siloxane reconstructed by combining the other subsector-optimized diel profiles.

mixing heights is 29.5 (−3.56) % in LV (LA). During night-time, lidar measurements of boundary layer height are much less frequently available and biases are on average −36.6 (46.4) % for LV (LA).

The selection of flights from the RECAP-CA campaign is based on the Pearson correlation coefficient for the water vapor mixing ratio between the model and aircraft measurements ($\rho > 0.6$). This criterion represents a trade-off between ensuring consistency in marine boundary layer representation in the basin and maintaining sufficient data for the inversion. Five flights (June 4, 10, 11, 12, and 21) were retained (flightpaths in SI, Figure S8), while 11 flights (June 1, 3, 6, 8, 9, 13, 15, 16, 18, 19, and 22) were omitted from the analysis. The accumulated footprints for the ground-site and airborne data are shown in the SI (Figure S7).

Diurnal Emissions. When optimizing the temporal emissions profiles for the subsector emission rates in VCP LA, distinctions are made between weekday versus weekend profiles. The number of days for each inversion ranges from 3 (LV weekend days) to 14 (LA weekday), and optimized profiles are normalized to 100% (normalization factors in SI Table S1). Prior uncertainty is set to 100% to allow for sufficiently large normalization factors and adapting the shape of the profile more freely. A second-order Fourier sum is fit to the combined data obtained from LA and LV optimized profiles in order to obtain a smooth curve (Figure 2) that reflects the general activity curve present in the inventory.

While the Lagrangian optimized profile shapes are mostly similar to the ones in the previous article, the D5-Siloxane diurnal emission profile changes starkly. During the week, D5-Siloxane emissions are at a minimum around 4–5 a.m. (3.1% of total 24 h emissions) and peak between noon and 1 p.m. (5.2%). The diurnal profile during the weekend shows a similar behavior, with a minimum of 3.0% at 4–5 a.m. and a maximum at 2 p.m. (5.7%). The amplitudes of D5-Siloxane and PDCBZ diel profiles are lower in the optimized result compared to the prior. For both tracers, the maxima occur later in the day during the weekend. In contrast to both D5-Siloxane and PDCBZ (tracers specific to consumer behavior), the optimal PCBTF (related to construction) profiles show larger differences between daytime (up to 9.4/8.3% for weekday/weekend) and night-time (minimum of 1.1/2.0% for weekday/weekend) emissions. Note also that the amplitudes of the PCBTF-optimized diel profiles are lower during the weekend than during the work week. From the normalization factors at both sites (Table S1), no obvious weekday-weekend effect is found in terms of total mass emitted daily for any of the subsectors.

Reconstructing the D4-Siloxane profile from a combination of the other tracers representing their respective sectors (i.e., 50% from construction, 47% from consumer, and 3% from insecticides; black dashed line in Figure 2) results in good agreement with the optimized D4-Siloxane profile with the difference never exceeding 1.0% of the daily emissions.

We remark that the diel profile for D5-Siloxane differs between LA and LV. Specifically, the LA-optimized diel profile shows a small peak in the morning (6 a.m.), followed by a decrease to a local minimum at 8 a.m., after which a sharp peak occurs from 11 a.m. to noon. In contrast, the LV diel profile peaks in the afternoon/evening, which may be consistent with the uniqueness of the LV strip. Here, we take both cities to fit a single diel profile in order to bound uncertainty in diel patterns of consumer VCP emissions. Differences between both sites may point to the need for regional activity profiles for consumer product emissions. As the prior D5-Siloxane diel profile was inferred from wintertime measurements in Boulder (CO) and measurements in May from Toronto (ON, CA), drivers in consumer behavior based on the region and climate could

https://doi.org/10.1021/acs.est.4c10117
Environ. Sci. Technol. 2025, 59, 7211−7221

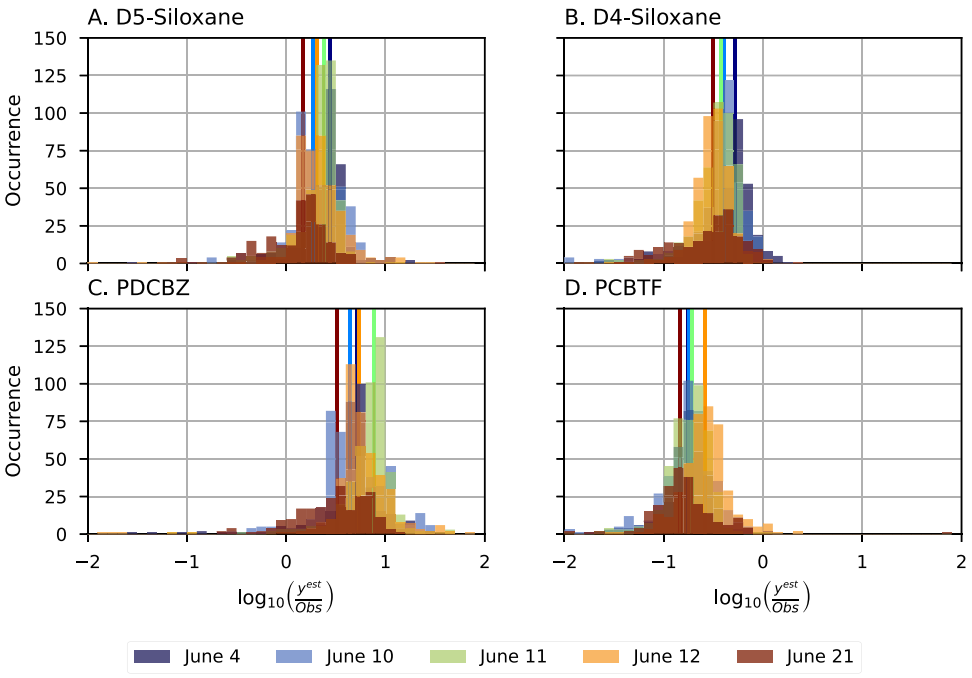

Figure 3. Distributions of the ratio between estimates combining the prior inventory with the calculated footprints (y^{est}) and the aircraft observations (Obs) for the VCP tracers (A, D5-Siloxane; B, D4-Siloxane; C, PDCBZ; D, PCBTF). Distributions from each flight during RECAP-CA are shown and color-coded by flight. Median values are shown by solid lines.

potentially explain the difference between the prior and posterior emission profile.

Note that the uncertainty in the optimized profiles relates predominantly to boundary layer representations in the model. We expect the night-time bias to compensate between the LA and LV optimizations, as they are similarly underestimating/overestimating the BL height, respectively. During the daytime, however, the boundary layer height in LV is overestimated by ~30% on average. This may indicate that the resulting optimized diel profile in LV overestimates the daytime emissions. Taking the LA emissions into account to fit the Fourier sum is expected to mediate this effect.

Top-Down VCP Emission Factors. Using the optimized diel profiles, we update the VCP LA inventory before calculating subsector regional EFs using the top-down approach. Figure 3 illustrates how subsector emission factors in the LA basin were adjusted using the RECAP-CA flights. The FLEXPART-WRF footprints are combined with the temporally optimized prior inventory to obtain model estimates (y^{est}) for the observed (Obs) mixing ratios using eq 1. We treat every flight as an independent observation and use the median value of $\frac{y^{est}}{Obs}$ as an estimate of the scaling factor (Figure 3). By using the ensemble of flights, we obtain an uncertainty on the scaling factor, which is considered to be representative of the uncertainty due to the transport model. The average scaling factors (±95% CI) combining the different flights are 2.10 ± 0.39, 0.39 ± 0.07, 5.16 ± 1.28, and 0.19 ± 0.03, for D5-Siloxane, D4-Siloxane, PDCBZ, and PCBTF, respectively. A scaling factor larger (smaller) than 1 implies that the inventory is estimated to be high (low). From this, we see that the inventory is estimated to be high for D5-Siloxane and PDCBZ, while low for D4-Siloxane and PCBTF.

To test the subsectoral consistency of our inverse modeling result, we estimate the D4-Siloxane emission rate (ER) by (1) using the prior EF and the D4-Siloxane scaling factor (74 mg person^{-1} day^{-1}), and (2) combining the top-down EFs for the consumer, construction, and insecticide subsectors (84 mg person^{-1} day^{-1}). The small (13%) difference between both builds confidence in the results of our approach. The top-down EFs derived from inverse modeling over the LA basin are shown in comparison with those from the literature in Figure 4. For completeness, we also included the EFs reported in McDonald et al.[1] on the national level, in addition to those that are LA-specific. Note that here we compare with the national EFs reported by Seltzer et al.[18] and Qin et al.[8] while the EFs from the

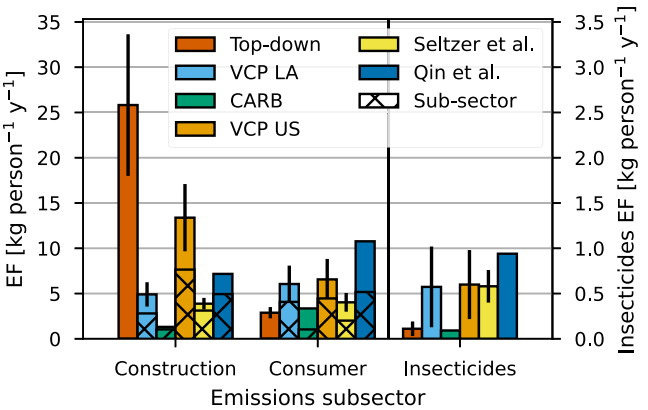

Figure 4. Top-down emission factors [kg person^{-1} year^{-1}] derived here (top-down) compared to EFs from McDonald et al.[1] (VCP US/VCP LA), Qin et al.,[8] Seltzer et al.,[18] and the inventory from the California Air Resources Board (CARB). The hatched fraction in inventory EFs for construction/consumer subsectors indicate the EF from coatings/personal care products, respectively. Error bars represent the 95% CI (Seltzer et al., top-down), expert uncertainty estimates (McDonald et al.[1]). Note that the insecticide subsector EFs are shown on a scale 1 order of magnitude smaller than the others.

https://doi.org/10.1021/acs.est.4c10117
Environ. Sci. Technol. 2025, 59, 7211−7221

California Air Resources Board (CARB) inventory are specific to the LA basin.

The total VOC emissions from the evaluated construction (coatings + adhesives), consumer (personal care + cleaning), and insecticide VCP sectors in the LA domain are higher from the top-down inventory (31 ± 8 kg person^{-1} year^{-1}) compared to all the bottom-up inventories. The bottom-up total VCP emissions range from 29% (VCP US) to 81% (CARB) lower compared to the top-down EFs. This is entirely due to the increased construction emissions (derived from the PCBTF tracer) which enhances emissions by a factor of 5.3 compared to the prior (VCP LA). The other subsectors (consumer and insecticides) are reduced after optimization.

While CARB, VCP LA, and Qin et al. estimate emissions from the consumer sector to be dominant over the construction emissions, the optimized EFs estimate that construction emissions are twice as large as those from consumers. VCP US is the only other inventory that estimates a higher EF from construction (9.7−17.1 kg person^{-1} year^{-1}) than from consumer products (4.30−8.84 kg person^{-1} year^{-1}). The construction EF in VCP US is also closest to the optimized results (18.0−33.6 kg person^{-1} year^{-1}). For both the consumer and insecticide sectors, the CARB inventory is closest to the top-down EFs, 2.3−3.5 and 0.0−0.2 kg person^{-1} year^{-1}, respectively. The top-down results are most in line with the VCP US inventory, as it is the only one that correctly estimates the dominant emissions related to construction in the basin in contrast to the consumer products and insecticides usage.

After using the top-down EFs to further correct the VCP LA inventory, we calculate its optimized spatial distribution of emission in the LA basin (Figure S9). For this, the uncertainty in the inventory corresponds to the uncertainty estimate on the optimized EFs. As we are using ∼1.9 k observations to optimize ∼5 k independent sources in the inventory, the individual emission rates are not considered here. However, we are able to discern the general features in the optimized result to identify regions that may need further study in the future. From this, we see that the different tracers are estimated to be low in the harbor region while those in more residential/commercial areas are high compared to the a posteriori result. Specifically, emissions of D5-Siloxane and PCBTF around the harbor region are increased with 29 and 10%, respectively. Further investigation on potential differences in emission patterns between industrial zones and residential areas may be needed to improve VCP inventories toward the future.

Above, we discussed the application of the scaling factors to obtain top-down optimized EFs and their uncertainties (combination of uncertainty in the inventory and uncertainty of the scaling factor). Alternatively, the scaling factors could be impacted by consistent biases in boundary layer height or measurements uncertainties. As we optimized the model performance for the region and selected flights to best reproduce the meteorological parameters, we attempted to minimize the meteorological bias and assume it to be small. Compounds calibrated directly with a gas standard (D4-, and D5-Siloxane) are not expected to be subject to a significant measurement bias. For PDCBZ and PCBTF, the scaling factors are outside the estimated measurement uncertainty (54%). As such, changes in the top-down EFs are assumed to be significant for all VCP subsectors.

We highlight the remaining discrepancies between bottom-up VCP inventories and our top-down evaluation. While VOC emissions from VCP consumer and insecticide subsectors were overestimated, emissions related to construction were underestimated by a factor of 5 and led to an overall underestimation of total VCP emissions. As the quantification of VCPs on criteria pollutants has been mostly based on bottom-up inventory estimates,[7−13] it is important to characterize uncertainties with top-down methodologies. The novel advance of this study is employing a Lagrangian modeling framework that rigorously accounts for meteorological transport in inverting emissions and revealed an under-accounted source of construction-related emissions, especially in industrial regions. Accurate representation of VOC reactivity in inventories is important for modeling the impact of urban emissions on tropospheric O_3 formation in Los Angeles,[13,27] and other cities around the world.[50]

■ ASSOCIATED CONTENT

Supporting Information

The Supporting Information is available free of charge at https://pubs.acs.org/doi/10.1021/acs.est.4c10117.

Additional details about the meteorological model selection, WRF-Chem configuration and comparison with stationary/mobile lidar data, FLEXPART-WRF configuration, data selection, and processing, and the spatial inversion. The VOC and lidar measurements used in this study are openly available and can be found here: https://csl.noaa.gov/projects/sunvex/ (last access 26 Aug 2024). The emission inventories used as prior optimization are available online (https://csl.noaa.gov/groups/csl7/measurements/2021sunvex/emissions/, last access 26 Aug 2024) (PDF)

■ AUTHOR INFORMATION

Corresponding Author

Bert W. D. Verreyken − *NOAA Chemical Sciences Laboratory, Boulder, Colorado 80304, United States;* Present Address: Royal Belgian Institute for Space Aeronomy (BIRA-IASB), Ukkel 1180, Belgium; Gembloux Agro-Biotech, Biosystems Dynamics and Exchanges (BIODYNE), University of Liège, Gembloux 5030, Belgium; orcid.org/0000-0002-5297-8524; Email: bert.verreyken@aeronomie.be

Authors

Colin Harkins − *NOAA Chemical Sciences Laboratory, Boulder, Colorado 80304, United States; Cooperative Institute for Research in Environmental Sciences (CIRES), University of Colorado Boulder, Boulder, Colorado 80309, United States;* orcid.org/0000-0001-5692-3427

Meng Li − *NOAA Chemical Sciences Laboratory, Boulder, Colorado 80304, United States; Cooperative Institute for Research in Environmental Sciences (CIRES), University of Colorado Boulder, Boulder, Colorado 80309, United States*

Wayne Angevine − *NOAA Chemical Sciences Laboratory, Boulder, Colorado 80304, United States; Cooperative Institute for Research in Environmental Sciences (CIRES), University of Colorado Boulder, Boulder, Colorado 80309, United States*

Chelsea E. Stockwell − *NOAA Chemical Sciences Laboratory, Boulder, Colorado 80304, United States; Cooperative Institute for Research in Environmental Sciences (CIRES), University of Colorado Boulder, Boulder, Colorado 80309, United States;* orcid.org/0000-0003-3462-2126

Lu Xu − *NOAA Chemical Sciences Laboratory, Boulder, Colorado 80304, United States; Cooperative Institute for*

Research in Environmental Sciences (CIRES), University of Colorado Boulder, Boulder, Colorado 80309, United States; Present Address: Department of Energy, Environmental and Chemical Engineering, Washington University, St. Louis, Missouri 63130, United States.; orcid.org/0000-0002-0021-9876

Matthew Coggon − *NOAA Chemical Sciences Laboratory, Boulder, Colorado 80304, United States;* orcid.org/0000-0002-5763-1925

Jessica Gilman − *NOAA Chemical Sciences Laboratory, Boulder, Colorado 80304, United States;* orcid.org/0000-0002-7899-9948

Carsten Warneke − *NOAA Chemical Sciences Laboratory, Boulder, Colorado 80304, United States;* orcid.org/0000-0003-3811-8496

Edward Strobach − *NOAA Chemical Sciences Laboratory, Boulder, Colorado 80304, United States; Cooperative Institute for Research in Environmental Sciences (CIRES), University of Colorado Boulder, Boulder, Colorado 80309, United States;* Present Address: University of Maryland College Park, College Park, Maryland 20742, United States.

Steven Brown − *NOAA Chemical Sciences Laboratory, Boulder, Colorado 80304, United States;* orcid.org/0000-0001-7477-9078

Brandi McCarty − *NOAA Chemical Sciences Laboratory, Boulder, Colorado 80304, United States; Cooperative Institute for Research in Environmental Sciences (CIRES), University of Colorado Boulder, Boulder, Colorado 80309, United States*

Richard Marchbanks − *NOAA Chemical Sciences Laboratory, Boulder, Colorado 80304, United States; Cooperative Institute for Research in Environmental Sciences (CIRES), University of Colorado Boulder, Boulder, Colorado 80309, United States*

Sunil Baidar − *NOAA Chemical Sciences Laboratory, Boulder, Colorado 80304, United States; Cooperative Institute for Research in Environmental Sciences (CIRES), University of Colorado Boulder, Boulder, Colorado 80309, United States*

Alan Brewer − *NOAA Chemical Sciences Laboratory, Boulder, Colorado 80304, United States*

Eva Y. Pfannerstill − *Department of Environmental Science, Policy, and Management, University of California, Berkeley, California 94720, United States;* Present Address: Institute for Climate and Energy Systems 3: Troposphere, Forschungszentrum Jülich, Jülich 52428, Germany.; orcid.org/0000-0001-7715-1200

Caleb Arata − *Department of Environmental Science, Policy, and Management, University of California, Berkeley, California 94720, United States*

Allen H. Goldstein − *Department of Environmental Science, Policy, and Management, University of California, Berkeley, California 94720, United States;* orcid.org/0000-0003-4014-4896

Jérome Brioude − *Laboratoire de l'Atmosphère et des Cyclones, UMR 8105, CNRS, Université de La Réunion, 97744 Saint-Denis, France*

Brian C. McDonald − *NOAA Chemical Sciences Laboratory, Boulder, Colorado 80304, United States;* orcid.org/0000-0001-8600-5096

Complete contact information is available at: https://pubs.acs.org/10.1021/acs.est.4c10117

Notes

The authors declare no competing financial interest.

■ ACKNOWLEDGMENTS

We acknowledge Clark County, Nevada Department of Environment & Sustainability, and the California Air Resources Board for providing support for SUNVEx measurements. The RECAP-CA field campaign was funded by California Air Resources Board 260 Contract number 20RD003, 20AQP012, and the Presidential Early Career Award for Scientists and Engineers (PECASE, from B.C.M.). We also acknowledge funding from the Cooperative Institute for Research in Environmental Sciences (grant nos. NA17OAR4320101 and NA22OAR4320151). We also thank NOAA's High Performance Computing Program. This research was performed while B.W.D.V. held an NRC Research Associateship award at NOAA CSL.

■ REFERENCES

(1) McDonald, B. C.; de Gouw, J. A.; Gilman, J. B.; Jathar, S. H.; Akherati, A.; Cappa, C. D.; Jimenez, J. L.; Lee-Taylor, J.; Hayes, P. L.; McKeen, S. A.; Cui, Y. Y.; Kim, S.-W.; Gentner, D. R.; Isaacman-VanWertz, G.; Goldstein, A. H.; Harley, R. A.; Frost, G. J.; Roberts, J. M.; Ryerson, T. B.; Trainer, M. Volatile Chemical Products Emerging as Largest Petrochemical Source of Urban Organic Emissions. *Science* **2018**, *359*, 760−764.

(2) Warneke, C.; De Gouw, J. A.; Holloway, J. S.; Peischl, J.; Ryerson, T. B.; Atlas, E.; Blake, D.; Trainer, M.; Parrish, D. D. Multiyear trends in volatile organic compounds in Los Angeles, California: Five decades of decreasing emissions: TRENDS IN VOCS IN LOS ANGELES. *J. Geophys. Res.: Atmos.* **2012**, *117*, No. D00V17.

(3) McDonald, B. C.; Gentner, D. R.; Goldstein, A. H.; Harley, R. A. Long-Term Trends in Motor Vehicle Emissions in U.S. Urban Areas. *Environ. Sci. Technol.* **2013**, *47*, 10022−10031.

(4) Gkatzelis, G. I.; Coggon, M. M.; McDonald, B. C.; Peischl, J.; Gilman, J. B.; Aikin, K. C.; Robinson, M. A.; Canonaco, F.; Prevot, A. S. H.; Trainer, M.; Warneke, C. Observations Confirm that Volatile Chemical Products Are a Major Source of Petrochemical Emissions in U.S. Cities. *Environ. Sci. Technol.* **2021**, *55*, 4332−4343.

(5) Brunet, C. E.; Marek, R. F.; Stanier, C. O.; Hornbuckle, K. C. Concentrations of Volatile Methyl Siloxanes in New York City Reflect Emissions from Personal Care and Industrial Use. *Environ. Sci. Technol.* **2024**, *58*, 8835−8845.

(6) Gkatzelis, G. I.; Coggon, M. M.; McDonald, B. C.; Peischl, J.; Aikin, K. C.; Gilman, J. B.; Trainer, M.; Warneke, C. Identifying Volatile Chemical Product Tracer Compounds in U.S. Cities. *Environ. Sci. Technol.* **2021**, *55*, 188−199.

(7) Coggon, M. M.; Gkatzelis, G. I.; McDonald, B. C.; Gilman, J. B.; Schwantes, R. H.; Abuhassan, N.; Aikin, K. C.; Arend, M. F.; Berkoff, T. A.; Brown, S. S.; Campos, T. L.; Dickerson, R. R.; Gronoff, G.; Hurley, J. F.; Isaacman-VanWertz, G.; Koss, A. R.; Li, M.; McKeen, S. A.; Moshary, F.; Peischl, J.; Pospisilova, V.; Ren, X.; Wilson, A.; Wu, Y.; Trainer, M.; Warneke, C. Volatile chemical product emissions enhance ozone and modulate urban chemistry. *Proc. Natl. Acad. Sci. U.S.A.* **2021**, *118*, No. e2026653118.

(8) Qin, M.; Murphy, B. N.; Isaacs, K. K.; McDonald, B. C.; Lu, Q.; McKeen, S. A.; Koval, L.; Robinson, A. L.; Efstathiou, C.; Allen, C.; Pye, H. O. T. Criteria pollutant impacts of volatile chemical products informed by near-field modelling. *Nat. Sustain.* **2021**, *4*, 129−137.

(9) Pennington, E. A.; Pennington, E. A.; Seltzer, K. M.; Murphy, B. N.; Qin, M.; Seinfeld, J. H.; Pye, H. O. T. Modeling secondary organic aerosol formation from volatile chemical products. *Atmos. Chem. Phys.* **2021**, *21*, 18247−18261.

(10) Abdi-Oskouei, M.; Roozitalab, B.; Stanier, C. O.; Christiansen, M.; Pfister, G.; Pierce, R. B.; McDonald, B. C.; Adelman, Z.; Janseen, M.; Dickens, A. F.; Carmichael, G. R. The Impact of Volatile Chemical Products, Other VOCs, and NO_x on Peak Ozone in the Lake Michigan Region. *J. Geophys. Res.: Atmos.* **2022**, *127*, No. e2022JD037042.

(11) Seltzer, K. M.; Murphy, B. N.; Pennington, E. A.; Allen, C.; Talgo, K.; Pye, H. O. T. Volatile Chemical Product Enhancements to Criteria

Pollutants in the United States. *Environ. Sci. Technol.* **2022**, *56*, 6905−6913.
(12) Sasidharan, S.; He, Y.; Akherati, A.; Li, Q.; Li, W.; Cocker, D.; McDonald, B. C.; Coggon, M. M.; Seltzer, K. M.; Pye, H. O. T.; Pierce, J. R.; Jathar, S. H. Secondary Organic Aerosol Formation from Volatile Chemical Product Emissions: Model Parameters and Contributions to Anthropogenic Aerosol. *Environ. Sci. Technol.* **2023**, *57*, 11891−11902.
(13) Stockwell, C. E.; Coggon, M. M.; Schwantes, R. H.; Harkins, C.; Verreyken, B.; Lyu, C.; Zhu, Q.; Xu, L.; Gilman, J. B.; Lamplugh, A.; Peischl, J.; Robinson, M. A.; Veres, P. R.; Li, M.; Rollins, A. W.; Zuraski, K.; Baidar, S.; Liu, S.; Kuwayama, T.; Brown, S. S.; McDonald, B. C.; Warneke, C. Urban ozone formation and sensitivities to volatile chemical products, cooking emissions, and NO_x upwind of and within two Los Angeles Basin cities. *Atmos. Chem. Phys.* **2025**, *25*, 1121−1143.
(14) McDonald, B. C.; McBride, Z. C.; Martin, E. W.; Harley, R. A. High-resolution mapping of motor vehicle carbon dioxide emissions: Motor Vehicle CO2 Emissions. *J. Geophys. Res.: Atmos.* **2014**, *119*, 5283−5298.
(15) Harkins, C.; McDonald, B. C.; Henze, D. K.; Wiedinmyer, C. A fuel-based method for updating mobile source emissions during the COVID-19 pandemic. *Environ. Res. Lett.* **2021**, *16*, No. 065018.
(16) Guenther, A. B.; Jiang, X.; Heald, C. L.; Sakulyanontvittaya, T.; Duhl, T.; Emmons, L. K.; Wang, X. The Model of Emissions of Gases and Aerosols from Nature version 2.1 (MEGAN2.1): an extended and updated framework for modeling biogenic emissions. *Geosci. Model Dev.* **2012**, *5*, 1471−1492.
(17) Peng, Y.; Mouat, A. P.; Hu, Y.; Li, M.; McDonald, B. C.; Kaiser, J. Source appointment of volatile organic compounds and evaluation of anthropogenic monoterpene emission estimates in Atlanta, Georgia. *Atmos. Environ.* **2022**, *288*, No. 119324.
(18) Seltzer, K. M.; Pennington, E.; Rao, V.; Murphy, B. N.; Strum, M.; Isaacs, K. K.; Pye, H. O. T. Reactive organic carbon emissions from volatile chemical products. *Atmos. Chem. Phys.* **2021**, *21*, 5079−5100.
(19) Pfannerstill, E. Y.; Arata, C.; Zhu, Q.; Schulze, B. C.; Woods, R.; Harkins, C.; Schwantes, R. H.; McDonald, B. C.; Seinfeld, J. H.; Bucholtz, A.; Cohen, R. C.; Goldstein, A. H. Comparison between Spatially Resolved Airborne Flux Measurements and Emission Inventories of Volatile Organic Compounds in Los Angeles. *Environ. Sci. Technol.* **2023**, *57*, 15533−15545.
(20) Coggon, M. M.; Stockwell, C. E.; Xu, L.; Peischl, J.; Gilman, J. B.; Lamplugh, A.; Bowman, H. J.; Aikin, K.; Harkins, C.; Zhu, Q.; Schwantes, R. H.; He, J.; Li, M.; Seltzer, K.; McDonald, B.; Warneke, C. Contribution of cooking emissions to the urban volatile organic compounds in Las Vegas, NV. *Atmos. Chem. Phys.* **2024**, *24*, 4289−4304.
(21) Coggon, M. M.; McDonald, B. C.; Vlasenko, A.; Veres, P. R.; Bernard, F.; Koss, A. R.; Yuan, B.; Gilman, J. B.; Peischl, J.; Aikin, K. C.; DuRant, J.; Warneke, C.; Li, S.-M.; De Gouw, J. A. Diurnal Variability and Emission Pattern of Decamethylcyclopentasiloxane (D_5) from the Application of Personal Care Products in Two North American Cities. *Environ. Sci. Technol.* **2018**, *52*, 5610−5618.
(22) Brioude, J.; Angevine, W. M.; Ahmadov, R.; Kim, S.-W.; Evan, S.; McKeen, S. A.; Hsie, E.-Y.; Frost, G. J.; Neuman, J. A.; Pollack, I. B.; Peischl, J.; Ryerson, T. B.; Holloway, J.; Brown, S. S.; Nowak, J. B.; Roberts, J. M.; Wofsy, S. C.; Santoni, G. W.; Oda, T.; Trainer, M. Top-down estimate of surface flux in the Los Angeles Basin using a mesoscale inverse modeling technique: assessing anthropogenic emissions of CO, NO_x and CO_2 and their impacts. *Atmos. Chem. Phys.* **2013**, *13*, 3661−3677.
(23) Karion, A.; Lauvaux, T.; Lopez Coto, I.; Sweeney, C.; Mueller, K.; Gourdji, S.; Angevine, W.; Barkley, Z.; Deng, A.; Andrews, A.; Stein, A.; Whetstone, J. Intercomparison of atmospheric trace gas dispersion models: Barnett Shale case study. *Atmos. Chem. Phys.* **2019**, *19*, 2561−2576.
(24) Angevine, W. M.; Peischl, J.; Crawford, A.; Loughner, C. P.; Pollack, I.; Thompson, C. R. Errors in Top-down Estimates of Emissions Using a Known Source. *Atmos. Chem. Phys.* **2020**, *20*, 11855−11868.
(25) Li, M.; McDonald, B. C.; McKeen, S. A.; Eskes, H.; Levelt, P.; Francoeur, C.; Harkins, C.; He, J.; Barth, M.; Henze, D. K.; Bela, M. M.; Trainer, M.; De Gouw, J. A.; Frost, G. J. Assessment of Updated Fuel-Based Emissions Inventories Over the Contiguous United States Using TROPOMI NO_2 Retrievals. *J. Geophys. Res.: Atmos.* **2021**, *126*, No. e2021JD035484.
(26) He, J.; Harkins, C.; O'Dell, K.; Li, M.; Francoeur, C.; Aikin, K. C.; Anenberg, S.; Baker, B.; Brown, S. S.; Coggon, M. M.; Frost, G. J.; Gilman, J. B.; Kondragunta, S.; Lamplugh, A.; Lyu, C.; Moon, Z.; Pierce, B. R.; Schwantes, R. H.; Stockwell, C. E.; Warneke, C.; Yang, K.; Nowlan, C. R.; González Abad, G.; McDonald, B. C. COVID-19 perturbation on US air quality and human health impact assessment. *PNAS Nexus* **2024**, *3*, No. pgad483.
(27) Zhu, Q.; Schwantes, R. H.; Stockwell, C. E.; Harkins, C.; Lyu, C.; Coggon, M.; Yu, K. A.; Warneke, C.; Schnell, J.; He, J.; Pye, H. O. T.; Li, M.; Ahmadov, R.; Pfannerstill, E. Y.; Place, B.; Wooldridge, P.; Schulze, B. C.; Arata, C.; Bucholtz, A.; Seinfeld, J. H.; Xu, L.; Zuraski, K.; Robinson, M. A.; Neuman, J. A.; Gilman, J.; Lamplugh, A.; Veres, P. R.; Peischl, J.; Rollins, A.; Brown, S. S.; Goldstein, A. H.; Cohen, R. C.; McDonald, B. C. Incorporating Cooking Emissions To Better Simulate the Impact of Zero-Emission Vehicle Adoption on Ozone Pollution in Los Angeles. *Environ. Sci. Technol.* **2025**, *59* (11), 5672−5682, DOI: 10.1021/acs.est.5c00902.
(28) Yu, K. A.; Li, M.; Harkins, C.; He, J.; Zhu, Q.; Verreyken, B.; Schwantes, R. H.; Cohen, R. C.; McDonald, B. C.; Harley, R. A. Improved Spatial Resolution in Modeling of Nitrogen Oxide Concentrations in the Los Angeles Basin. *Environ. Sci. Technol.* **2023**, *57*, 20689−20698, DOI: 10.1021/acs.est.3c06158.
(29) Janjic, Z.; Gall, R. *Scientific Documentation of the NCEP Nonhydrostatic Multiscale Model on the B Grid (NMMB). Part 1 Dynamics*, 2012.
(30) Benjamin, S. G.; Weygandt, S. S.; Brown, J. M.; Hu, M.; Alexander, C. R.; Smirnova, T. G.; Olson, J. B.; James, E. P.; Dowell, D. C.; Grell, G. A.; Lin, H.; Peckham, S. E.; Smith, T. L.; Moninger, W. R.; Kenyon, J. S.; Manikin, G. S. A North American Hourly Assimilation and Model Forecast Cycle: The Rapid Refresh. *Mon. Weather Rev.* **2016**, *144*, 1669−1694.
(31) Nakanishi, M.; Niino, H. Development of an Improved Turbulence Closure Model for the Atmospheric Boundary Layer. *J. Meteorol. Soc. Jpn. Ser. II* **2009**, *87*, 895−912.
(32) Olson, J. B.; Kenyon, J. S.; Angevine, W. A.; Brown, J. M.; Pagowski, M.; Sušelj, K. A Description of the MYNN-EDMF Scheme and the Coupling to Other Components in WRF−ARW; Earth System Research Laboratory (U.S.), Global Systems Division, 2019.
(33) Kusaka, H.; Kimura, F. Coupling a Single-Layer Urban Canopy Model with a Simple Atmospheric Model: Impact on Urban Heat Island Simulation for an Idealized Case. *J. Meteorol. Soc. Jpn. Ser. II* **2004**, *82*, 67−80.
(34) Stohl, A.; Forster, C.; Frank, A.; Seibert, P.; Wotawa, G. Technical note: The Lagrangian particle dispersion model FLEXPART version 6.2. *Atmos. Chem. Phys.* **2005**, *5*, 2461−2474.
(35) Brioude, J.; Arnold, D.; Stohl, A.; Cassiani, M.; Morton, D.; Seibert, P.; Angevine, W.; Evan, S.; Dingwell, A.; Fast, J. D.; Easter, R. C.; Pisso, I.; Burkhart, J.; Wotawa, G. The Lagrangian Particle Dispersion Model FLEXPART-WRF Version 3.1. *Geosci. Model Dev.* **2013**, *6*, 1889−1904.
(36) Verreyken, B.; Brioude, J.; Evan, S. Development of Turbulent Scheme in the FLEXPART-AROME v1.2.1 Lagrangian Particle Dispersion Model. *Geosci. Model Dev.* **2019**, *12*, 4245−4259.
(37) Brioude, J.; Angevine, W. M.; McKeen, S. A.; Hsie, E.-Y. Numerical uncertainty at mesoscale in a Lagrangian model in complex terrain. *Geosci. Model Dev.* **2012**, *5*, 1127−1136.
(38) Seibert, P.; Frank, A. Source-receptor matrix calculation with a Lagrangian particle dispersion model in backward mode. *Atmos. Chem. Phys.* **2004**, *4*, 51−63.
(39) McDonald, B. C.; McKeen, S. A.; Cui, Y. Y.; Ahmadov, R.; Kim, S.-W.; Frost, G. J.; Pollack, I. B.; Peischl, J.; Ryerson, T. B.; Holloway, J. S.; Graus, M.; Warneke, C.; Gilman, J. B.; De Gouw, J. A.; Kaiser, J.; Keutsch, F. N.; Hanisco, T. F.; Wolfe, G. M.; Trainer, M. Modeling

Ozone in the Eastern U.S. using a Fuel-Based Mobile Source Emissions Inventory. *Environ. Sci. Technol.* **2018**, *52*, 7360−7370.
(40) Coggon, M. M.; Stockwell, C. E.; Claflin, M. S.; Pfannerstill, E. Y.; Xu, L.; Gilman, J. B.; Marcantonio, J.; Cao, C.; Bates, K.; Gkatzelis, G. I.; Lamplugh, A.; Katz, E. F.; Arata, C.; Apel, E. C.; Hornbrook, R. S.; Piel, F.; Majluf, F.; Blake, D. R.; Wisthaler, A.; Canagaratna, M.; Lerner, B. M.; Goldstein, A. H.; Mak, J. E.; Warneke, C. Identifying and correcting interferences to PTR-ToF-MS measurements of isoprene and other urban volatile organic compounds. *Atmos. Meas. Tech.* **2024**, *17*, 801−825.
(41) Bonin, T. A.; Carroll, B. J.; Hardesty, R. M.; Brewer, W. A.; Hajny, K.; Salmon, O. E.; Shepson, P. B. Doppler Lidar Observations of the Mixing Height in Indianapolis Using an Automated Composite Fuzzy Logic Approach. *J. Atmos. Ocean. Technol.* **2018**, *35*, 473−490.
(42) Schroeder, P.; Brewer, W. A.; Choukulkar, A.; Weickmann, A.; Zucker, M.; Holloway, M. W.; Sandberg, S. A Compact, Flexible, and Robust Micropulsed Doppler Lidar. *J. Atmos. Ocean. Technol.* **2020**, *37*, 1387−1402.
(43) Pfannerstill, E. Y.; Arata, C.; Zhu, Q.; Schulze, B. C.; Woods, R.; Seinfeld, J. H.; Bucholtz, A.; Cohen, R. C.; Goldstein, A. H. Volatile organic compound fluxes in the agricultural San Joaquin Valley − spatial distribution, source attribution, and inventory comparison. *Atmos. Chem. Phys.* **2023**, *23*, 12753−12780.
(44) Zhu, Q.; Place, B.; Pfannerstill, E. Y.; Tong, S.; Zhang, H.; Wang, J.; Nussbaumer, C. M.; Wooldridge, P.; Schulze, B. C.; Arata, C.; Bucholtz, A.; Seinfeld, J. H.; Goldstein, A. H.; Cohen, R. C. Direct observations of NO_x emissions over the San Joaquin Valley using airborne flux measurements during RECAP-CA 2021 field campaign. *Atmos. Chem. Phys.* **2023**, *23*, 9669−9683.
(45) Pfannerstill, E. Y.; Arata, C.; Zhu, Q.; Schulze, B. C.; Ward, R.; Woods, R.; Harkins, C.; Schwantes, R. H.; Seinfeld, J. H.; Bucholtz, A.; Cohen, R. C.; Goldstein, A. H. Temperature-dependent emissions dominate aerosol and ozone formation in Los Angeles. *Science* **2024**, *384*, 1324−1329.
(46) Krechmer, J.; Lopez-Hilfiker, F.; Koss, A.; Hutterli, M.; Stoermer, C.; Deming, B.; Kimmel, J.; Warneke, C.; Holzinger, R.; Jayne, J.; Worsnop, D.; Fuhrer, K.; Gonin, M.; De Gouw, J. Evaluation of a New Reagent-Ion Source and Focusing Ion−Molecule Reactor for Use in Proton-Transfer-Reaction Mass Spectrometry. *Anal. Chem.* **2018**, *90*, 12011−12018.
(47) Cappellin, L.; Karl, T.; Probst, M.; Ismailova, O.; Winkler, P. M.; Soukoulis, C.; Aprea, E.; Märk, T. D.; Gasperi, F.; Biasioli, F. On Quantitative Determination of Volatile Organic Compound Concentrations Using Proton Transfer Reaction Time-of-Flight Mass Spectrometry. *Environ. Sci. Technol.* **2012**, *46*, 2283−2290.
(48) Brioude, J.; Kim, S.-W.; Angevine, W. M.; Frost, G. J.; Lee, S.-H.; McKeen, S. A.; Trainer, M.; Fehsenfeld, F. C.; Holloway, J. S.; Ryerson, T. B.; Williams, E. J.; Petron, G.; Fast, J. D. Top-down estimate of anthropogenic emission inventories and their interannual variability in Houston using a mesoscale inverse modeling technique. *J. Geophys. Res.: Atmos.* **2011**, *116*, No. D20305.
(49) Fletcher, S. J.; Zupanski, M. A data assimilation method for log-normally distributed observational errors. *Q. J. R. Meteorol. Soc.* **2006**, *132*, 2505−2519.
(50) Bauwens, M.; Verreyken, B.; Stavrakou, T.; Müller, J.-F.; Smedt, I. D. Spaceborne evidence for significant anthropogenic VOC trends in Asian cities over 2005−2019. *Environ. Res. Lett.* **2022**, *17*, No. 015008.

https://doi.org/10.1021/acs.est.4c10117
Environ. Sci. Technol. 2025, 59, 7211−7221